Hindawi
Wireless Communications and Mobile Computing
Volume 2023, Article ID 4889549, 18 pages
https://doi.org/10.1155/2023/4889549

Research Article

An Approach for Three-Dimensional Sectorization in the Terminal Area Based on Airspace Function

Lili Wan,[1] **Wenjing Ye**,[1] **Can Xu**,[1] **Jiangchen Li**,[1] **Xiao Huang**,[1] **Wenjian Gong**,[2] **and Yong Tian**[1]

[1]*College of Civil Aviation, Nanjing University of Aeronautics and Astronautics, Nanjing 210016, China*
[2]*East Regional Civil Aviation Administration of China, Shanghai 200335, China*

Correspondence should be addressed to Can Xu; xucan@nuaa.edu.cn

Received 6 October 2022; Revised 7 November 2022; Accepted 25 April 2023; Published 24 May 2023

Academic Editor: Shaohua Wan

As explainable artificial intelligence (XAI) has grown in popularity, it has become possible to more clearly explain the functional correspondence between airspace and traffic flow, which can alleviate the contradiction between the continuously increasing traffic demand in the terminal area and the limited airspace capacity; this paper studies the three-dimensional sectorization in the terminal area based on the airspace function. First, trajectory clustering is adopted to classify the functions of air traffic flows. Then, a functional sectorization framework is proposed to enable different airspace sectors with varied functions, where specifically the functional consistency objective between the airspace sector and the traversed air traffic flows is proposed. Third, a corresponding efficient algorithm is designed to generate functional sectors with an accurate scope that can well separate different traffic flows. Finally, the proposed method is evaluated by the actual operation datasets in the Shanghai terminal area. The results show that the method proposed in this paper can not only generate three-dimensional sectors with specific functions according to the prevailing traffic flow in the complex terminal area, which is conducive to the construction of controllers' situational awareness, but also can reduce potential conflicts and traffic density variance, increasing average sector flight time a lot.

1. Introduction

According to the 2016-2030 Global Air Navigation Plan published by the International Civil Aviation Organization (ICAO) in 2016, the civil aviation industry directly or indirectly contributes both 58.1 million jobs and 2.4 trillion dollars to the global gross domestic product [1]. However, with the further development of the civil aviation transportation system, the contradiction between the existing airspace capacity and the steady growing traffic demand intensities has extruded [2, 3]. The terminal area (TMA) is one key area that connects the airspace and the ground and guarantees the safe operations of landing, take off, and overflying flights. For a crowded TMA, the dense arrival and departure paths, narrow maneuvering room, and high flight density are striking features. To avoid flight conflicts in TMAs, enhancing human interaction and modifying the altitude, speed, and heading of aircraft are required. The process of human interaction is further referred to as the radar vectoring of aircraft by an air traffic controller (ATC). The workload of the ATC will reach a critical level when the authorized traffic flows are diverse and complex [4].

The airspace under one ATC's authority is a sector. Then, the airspace sectorization is partitioning the entire airspace into different sectors according to traffic flows, air routes and waypoints, and conflict distributions. It is a key aspect of the planning and management of airspace resource allocation. Currently, the majority of sectors are planned using some common principles outlined in the ICAO documents [5–7] and combined with expertise. However, its subjective component leads to some irrational allocation drawbacks of airspace resources, resulting in many potential conflicts, and limited sector capacity [8].

Extensive studies have been conducted to examine the scientific sectorization strategy, where they are evolving

from two-dimensional (2D) sectorization into three-dimensional (3D) sectorization, even into the most recent dynamic airspace sectorization (DAS). The focus of the current research is on the optimization of ATC's workloads, which suffers a lack of a standardized quantification. The sectors of these traditional studies frequently cover various types of traffic flows in space but have no defined function. The purpose of explainable artificial intelligence (EAI) is to enable artificial intelligence (AI) to interpret the results of its decisions in a way that can be understood by humans. In the area of air traffic management, in order to accomplish this goal, this work proposes an airspace function-driven three-dimensional sectorization methodology to generate sectors where its operating functions are consistent with traversed traffic flow functions. This methodology can better explain the functional correspondence between airspace and traffic flow, and functional sectors generated by this methodology demonstrate the interpretability of the results. The contribution of this work is shown as follows:

(1) This paper is the first one to clarify the function of air traffic flows and airspace sectors and provide a functional sectorization framework to enable different airspace sectors with varied functions, where specifically the functional consistency objective between the airspace sectors and air traffic flows is proposed. The air traffic flow classification results by the DBSCAN clustering fit with the actual operational process of the controller's perception, reflecting the interpretability of artificial intelligence

(2) An efficient functional sectorization algorithm is proposed to generate functional sectors with accurate horizontal and vertical ranges, where the corresponding initial generation rule, judgment and adjustment rule, gap-filling rule, and optimization process are designed to well separate different traffic flows. This algorithm can naturally satisfy the constraint on the one hand, and the running time is very short on the other hand

(3) The actual operation datasets of a typical complex TMA are utilized to evaluate the functional sectorization framework and algorithm. To conduct a comparison between the current and proposed functional sectors, performance indicators are chosen to measure sector benefits

The main contents of this paper are organized as follows. Section 2 classifies the function of the traffic flow by trajectory clustering. In Section 3, a framework of functional sectorization is proposed in the form of discretizing the TMA into several 3D airspace cells. Then, Section 4 designs corresponding algorithms with specific rules according to the framework of functional sectorization. Next, Section 5 uses actual operation datasets of the Shanghai TMA to evaluate the effectiveness of the functional sectors. Last, Section 6 draws conclusions from this study.

2. Literature Review and the Methodology Overview

Many academics have been working on reasonable sectorization methods. Early in 1994, Delahaye et al. used the Voronoi diagram to balance the ATCs' monitoring workload and reduce the coordination workload. However, constraints were not sufficiently considered resulting in the generated sector being less practical [9, 10]. Han and Zhang proposed a transformed Voronoi diagram of airspace, which can better guarantee operational safety but failed to achieve other constraints as well [11]. Following that, Yousefi and Donohue and Klein used mixed integer programming (MIP) in airspace sectorization to better satisfy the connectivity constraint and convex constraint [12, 13]. In 2009, Brinton et al. suggested the novel notion of using aircraft trajectories as the major research goal and generating sectors based on clustering results [14]. In 2010, Bloem and Gupta applied the dynamic programming method to tackle the airspace sectorization [15]. In 2013, Jagare et al. designed a constrained local search algorithm to drastically cut computing time [16]. Then, Zenlinski evaluated and summarized the advantages and limitations of the three methods of the Voronoi diagram, MIP, and trajectory clustering in 2016 [17]. The above works are categorized as the sectorization of the 2D plane and lack vertical altitude partitions. At the same time, altitude is one of the important parameters of aircraft motion and should not be ignored [18].

On the basis of one prior research, Delahaye and Puechmorel split the flight levels to form 3D airspace cells in 2008, and the right prism constraint was imposed to 3D sectorization [18]. Kicinger and Yousefi divided the airspace into cube cells in 2009 and then generated sectors using the agent-based model (ABM), which has good optimization efficiency but is easy to construct nested sectors [19]. Following that, Tang et al. proposed an improved ABM, which can better satisfy the relevant constraints [20, 21]. Xue presented a 3D sectorization method to optimize the number of sectors in 2012 [22]. Wei et al. proposed the optimization object of splitting arrival and departure traffic flow into separate sectors, which addresses a real requirement among controllers. However, because the flight procedure in the Atlanta TMA has completed the separation of arrival and departure, this strategy is insufficient for TMAs where arrival and departure flight procedures have significantly crossed [23]. Sergeeva et al. used a genetic algorithm to improve 3D sectors in 2015 [24]. Yin et al. generated 3D sectors for the en-route airspace of Singapore in 2016 [25]. Schmidt et al. suggested a new MIP-based sectorization method in 2017 that can naturally meet a variety of constraints [26]. Granberg et al. used the Stockholm Arlanda TMA as a case study in 2019 to develop a paradigm for extremely flexible sectorization [27]. Oktal et al. used CPLEX to solve the best sectorization for Turkish en-route airspace in 2020 [28]. Although the vertical height division is taken into account in the research, it is normally done first, followed by the horizontal height division, which simplifies the 3D problem to the 2D problem [8].

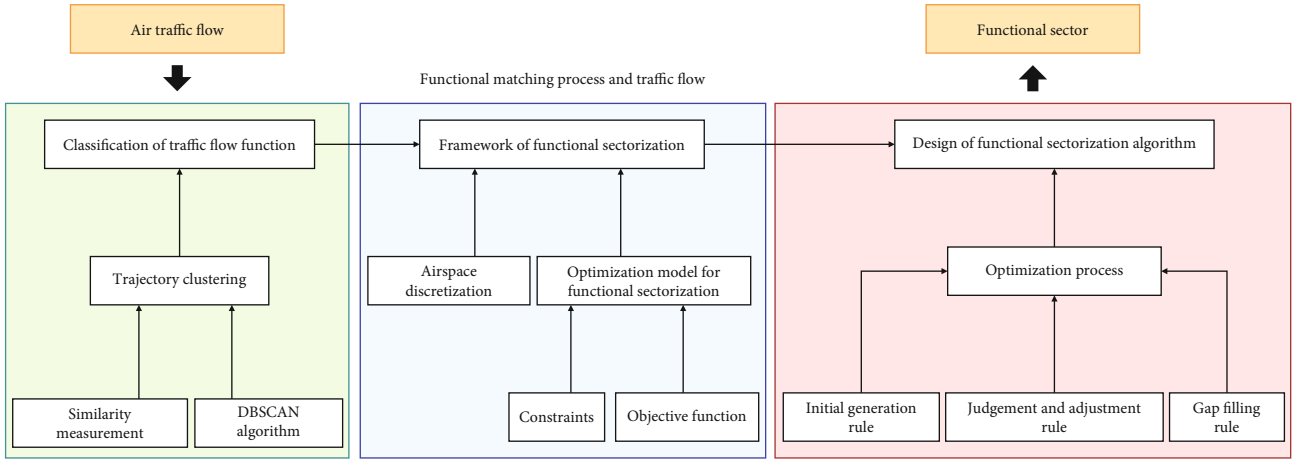

Figure 1: An airspace function-driven 3D sectorization methodology.

Furthermore, DAS has gradually become a hotspot of research. The DAS was originally proposed by Kopardekar et al.'s work in 2007 [29]. The DAS was then performed by Martinez et al., Sabhnani and Martin, and Chen et al. as traffic flow changed [30–32]. Schultz et al. conducted a DAS research study in 2017 with the purpose of balancing traffics among different sectors [33]. To execute a DAS strategy, Venugopalan et al. presented a bar graph-cut approach in 2018 [34]. In the same year, Gerdes et al. realized DAS centered on traffic flow [35]. Wong et al. suggested an approach that takes the next hour's flow into account [36] and proposed the rolling optimization approach for the gradient of sectors in 2020 [37]. DAS is a very popular concept in sectorization in recent years but with many controversies. Many people think that the DAS concept is unworkable because ATC will require enough time to adjust to the new sector shape [37]. In addition, DAS also needs to be based on accurate flow prediction results, which is difficult in all fields [38, 39], including air traffic management. This study does not go into great detail about this; instead, it concentrates on how to identify the main traffic flow of a given operating scene and construct functional sectors that match it.

Overall, the 2D sectorization cannot reflect the important altitude characteristics of traffic flow, while DAS is not developed sufficiently, and this paper's research is not focused on it, so 3D sectorization is the most suitable research method for this paper. What is more, the various existing studies mainly focused on how to optimize ATCs' workload, and to the best of our knowledge, no studies have been undertaken with the optimization objective of generating sectors where its operating functions are consistent with traversed traffic flows functions. Besides, most studies focus on the en-route airspace, and few focus on the TMA. In comparison to en-route airspace, many aircraft must take off or land in the TMA, which causes frequent altitude changes in a short amount of time. While the vertical height is frequently simply split and combined before the horizontal partitioning in current 3D sectorization, this process results in a very rough vertical range of the generated sector and thus can be further improved. Last but not least, the existing studies on sectorization in the TMA rarely consider multiairport TMA and overflying flights.

The purpose of this work is to investigate the 3D sectorization focusing on the airspace and sector function in the TMA. The overall methodology is introduced by three components, as shown in Figure 1. First, the functions of air traffic flow are classified using the trajectory clustering method. After that, the framework of functional sectorization is built. Finally, the functional sectorization algorithm is designed.

3. Classification of Traffic Flow Function

Classification of traffic flow function lays a foundation for the framework of functional sectorization. Air traffic trajectory data is discrete, has unequal numbers of tracks, and has different starting and ending points, so the DBSCAN method is effective for its advantages of being able to discover clusters of arbitrary shapes and not requiring the number of clusters to be set a priori. We continuously adjust the parameters according to the actual traffic flow, and trajectories with different operation modes and function and airspace requirements are divided.

3.1. Trajectory Description. The space-air-ground integrated network(SAGIN) is considered to be a significant framework for realizing the vision of the "6G intelligent connection of all things" [40, 41]. The software-defined network (SDN) data plane was composed of space-based, air-based, and ground-based networks. The operation status of aircraft in the TMA is primarily recorded by the air-based and ground-based networks, such as the primary radar, the secondary radar, and the automatic dependent surveillance-broadcast. Because of the signal's stability, the secondary radar is most widely used. This study uses secondary radar data with an update rate from 4 to 10 seconds. Each update produces a record containing longitude, latitude, altitude, speed, heading, and other aircraft data, which is then merged with the update time to generate complete four-dimensional (4D) trajectories. Figure 2 depicts these flight trajectories within a typical TMA during a peak hour. From the flight trajectories in Figure 2, we can not only find the application

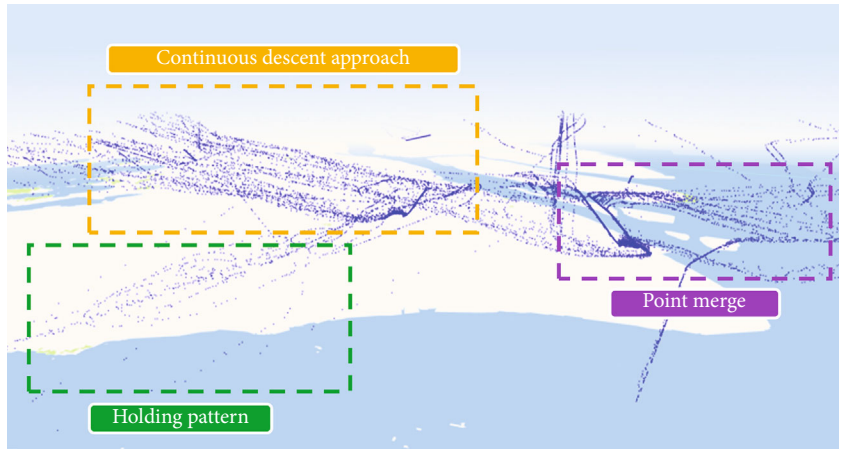

Figure 2: Flight trajectories within a typical TMA during a peak hour.

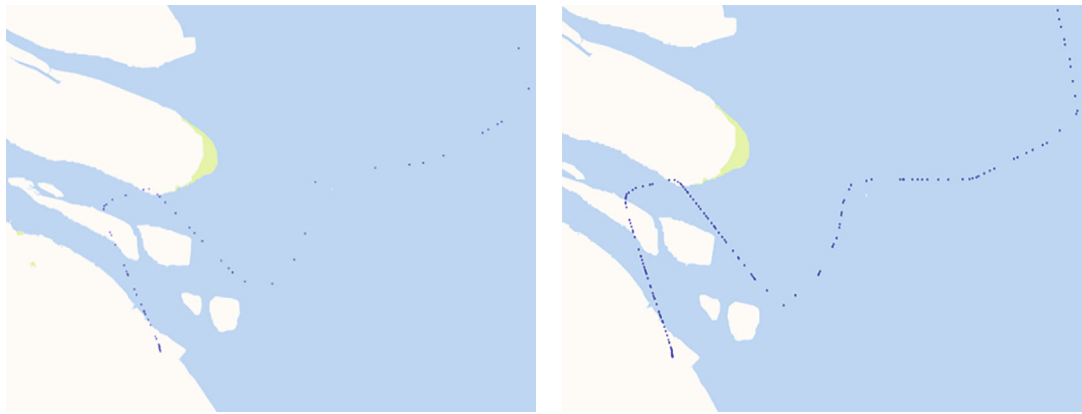

(a) Before resampling (b) After resampling

Figure 3: One trajectory example before and after the resampling.

of some traditional holding pattern but also see some new flight procedures, such as of point merge system (PMS) and continuous descent approach (CDA).

Considering that the motion parameters of the aircraft do not change drastically in a short period of time, the data can be resampled by an interpolation method, which enables the replenishment of key waypoints, facilitating the subsequent calculation. This study set the interval as 5 s by experimental comparisons, and one trajectory example before and after the resampling is shown in Figure 3.

3.2. Trajectory Clustering. In a typical TMA operation scenario, the number of aircraft in the TMA during a certain period of time is denoted as m, and the set of trajectories is denoted as C:

$$C = \{P_1, P_2, \cdots, P_m\}, \tag{1}$$

where P_i is the ith trajectory consisting of n_i points, which are lined up in chronological order.

$$P_i = \left\{p_{i,1}, p_{i,2}, \cdots, p_{i,n_i}\right\}, \tag{2}$$

where $p_{i,j}$ is the jth point of the ith trajectory and $j \in \{1, n_i\}$. Each point can be represented by a six-dimensional vector:

$$p_{i,j} = \{x, y, h, d, e, t\}, \tag{3}$$

where x, y, h, d, e, and t are the latitude, longitude, altitude, heading, speed, and update time, respectively.

The characteristics of aircraft operation dictate that close trajectories tend to have more similar operation modes, which are referred to as functions in this paper. We use trajectory clustering to divide the set of trajectories into K subsets by distinguishing the similarity between trajectories. Each cluster has a consistent function inside.

$$C = \{c_1, c_2, \cdots, c_K\}, \tag{4}$$

where C denotes the set of trajectories and c_i denotes the ith cluster, which consists of m_i trajectories.

$$c_i = \left\{P_1, P_2, \cdots, P_{m_i}\right\}. \tag{5}$$

The clusters do not intersect with each other, and each flight trajectory belongs to only one cluster, i.e., the

following equation is satisfied:

$$\begin{aligned} c_1 \cup c_2 \cdots \cup c_K &= C, \\ c_i \cap c_j &= \varnothing (1 \le i, j \le K, i \ne j). \end{aligned} \tag{6}$$

The distance between different trajectories varies depending on the chosen similarity factor, which is denoted as $d_{P_i,P_j}\ (1 \le i, j \le m)$. The sum of the distances for all clusters is calculated by

$$D(c, u) = \sum_{i=1}^{m} d\left(P_i, u_{c_i}\right) \tag{7}$$

where P_i is the ith trajectory, c_i is the cluster to which the ith trajectory belongs, and u_{c_i} is the center of the cluster. It is required to solve the division scheme C to minimize $D(c, u)$.

3.2.1. Similarity Measurement. In order to solve the division scheme C, an appropriate distance measurement must be chosen to appropriately describe the similarity of aircraft trajectories. In this paper, we adopt the Euclidean distance of adjacent trajectory points as the similarity measurement.

Take arrival trajectories P_i and P_j as examples, the set of trajectory points are $P_i = \{p_{i,1}, p_{i,2}, \cdots, p_{i,n_i}\}$ and $P_j = \{p_{j,1}, p_{j,2}, \cdots, p_{j,n_j}\}$, respectively. Because each trajectory has a different number of points, this study calculates the distance between two trajectories by comparing point-by-point along the opposite direction. The following is the process of calculating the distance between two trajectories, as shown in Figure 4.

3.2.2. Clustering Process. Based on the distance matrix, the clustering algorithm can then be used to cluster the trajectories. The DBSCAN algorithm offers the advantages of being able to discover clusters of any shape and not requiring a preset number of clusters, as well as being able to distinguish between core points and noise [42]. The data of aircraft trajectory contains irregular distribution, many anomalous data, and aggregation based on operation patterns, making it ideal for clustering using the DBSCAN algorithm.

During the operation of the DBSCAN algorithm, it is essential to set the values of parameters eps and min_samples. Figure 5 shows the effect of different parameter settings on the clustering results, where the solid points are the points belonging to the clusters, different clusters are distinguished by different colors, and the empty points are the noise.

4. Framework of Functional Sectorization

The goal of functional sectorization is, firstly, to satisfy the various constraints of traditional sectorization to ensure the scheme's practicality and, secondly, to make each sector cover a mainstream traffic flow as much as possible, so that the function of the sector matches the function of the traffic flow.

4.1. Airspace Discretization. The TMA is discretized into numerous cuboid cells, and the function of each cell is determined by the function of the trajectories passing through the cell. As a result, the TMA can be written as

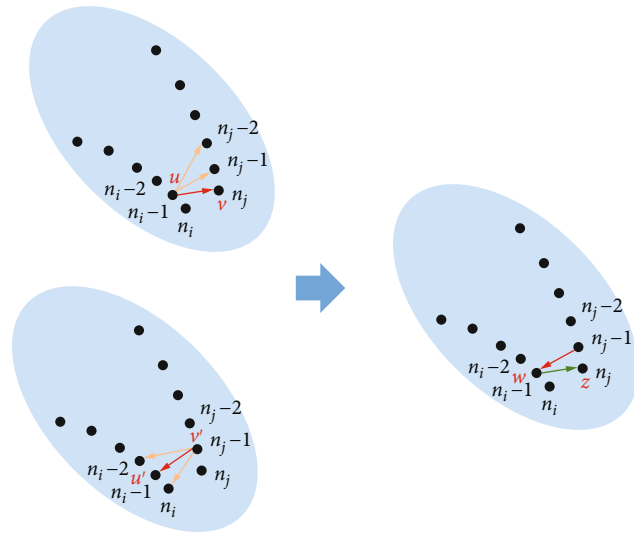

Figure 4: Process of calculating the distance between two trajectories.

$$R = \bigcup_{u,v,z} L\left(P'\right)_{\text{uvz}}, \tag{8}$$

where R is the whole TMA. $L(P')_{\text{uvz}}$ is one cuboid cell in the TMA, and $P' = \{p_{i_1,j_1}, p_{i_2,j_2}, \cdots, p_{i_n,j_n}\}\ (1 \le i_t \le m, 1 \le j_t \le n_{i_t})$ is the set of trajectory points contained in the cell. u, v, and z are the longitude, latitude, and altitude indices of the cell, which can be calculated by

$$\begin{aligned} u &= \frac{\text{lng} - \text{minLng}}{\text{lngSize}} + 1, \\ v &= \frac{\text{lat} - \text{minLat}}{\text{latSize}} + 1, \\ z &= \frac{\text{alt} - \text{minAlt}}{\text{altSize}} + 1, \end{aligned} \tag{9}$$

where lng, lat, and alt are the longitude, latitude, and altitude of the center point of the bottom surface of the cell. minLng, minLat, and minAlt are the minimum of longitude, latitude, and altitude of all cells. lngSize, latSize, and altSize are the predefined parameters that represent the size of the cell.

According to the trajectory clustering result in Section 3, the set of trajectories after clustering is denoted as $C = \{c_1, c_2, \cdots, c_K\}$, where $c_i = \{P_1, P_2, \cdots, P_{m_i}\}$. K functional sectors are generated based on K clusters of trajectories. Any functional sector can be denoted as S_k, $k = 1, 2, \cdots, K$. Combined with airspace discretization, we can define the function of airspace cell as follows:

$$\left(L\left(P'\right)_{\text{uvz}}, k\right) = \begin{cases} 1, \text{when} \exists p_{i_t,j_t} \in P', P_{i_t} \in c_k, \\ 0, \text{when} \forall p_{i_t,j_t} \in P', P_{i_t} \notin c_k. \end{cases} \tag{10}$$

For the cell $L(P')_{\text{uvz}}$, if it is passed through by trajectories

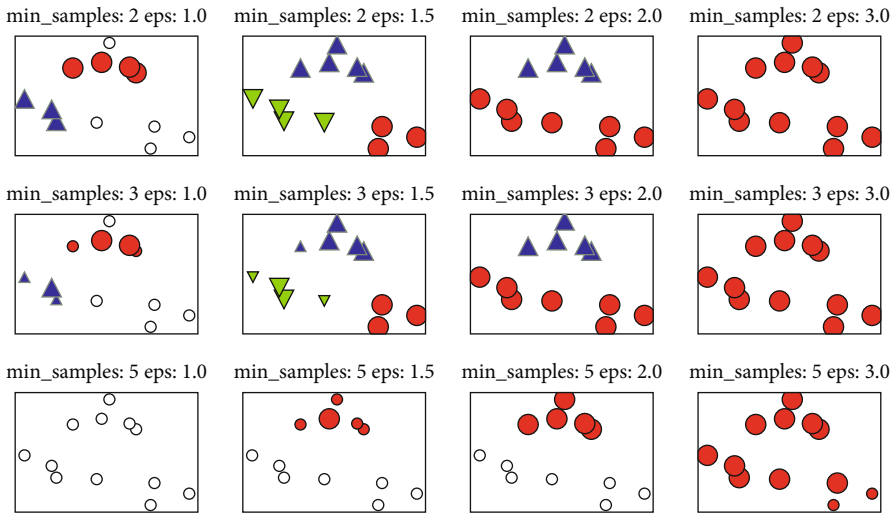

Figure 5: Clustering results obtained by different parameter settings.

of cluster k, the cell is considered to have the function of the trajectories of cluster k; otherwise, it does not. Cells that do not contain any trajectory point are blank. A cell can have multiple functions if it is passed through by multiple clusters of trajectories, and a blank cell does not have any function.

In order to generate a more precise range of sectors to better meet functional requirements, this paper further divides each sector into subsectors $S_{k,g}(k = 1, 2, \cdots, K\,; g = 1, \cdots, s_k)$, where s_k is the number of subsectors contained in the sector S_k, $1 \le s_k \le 3$. Considering that the sector should be a closed space, which is described in Section 4.2.2 as a connectivity constraint, this paper defines any subsector except boundary cells as a regular cuboid, which can be uniquely determined by a six-tuple $\mathrm{Six}(S_{k,g})$:

$$\begin{aligned} \mathrm{Six}\left(S_{k,g}\right) &= \left\{u_{\mathrm{left}}, u_{\mathrm{right}}, v_{\mathrm{back}}, v_{\mathrm{front}}, z_{\mathrm{bottom}}, z_{\mathrm{top}}\right\}, \\ 1 &\le u_{\mathrm{left}}, u_{\mathrm{right}} \le u_{\max}, \\ v_{\min}\left(u_{\mathrm{left}}, u_{\mathrm{right}}\right) &\le v_{\mathrm{back}}, v_{\mathrm{front}} \le v_{\max}\left(u_{\mathrm{left}}, u_{\mathrm{right}}\right), \\ 1 &\le z_{\mathrm{bottom}}, z_{\mathrm{top}} \le z_{\max}, \end{aligned} \tag{11}$$

where u_{left}, u_{right}, v_{front}, v_{back}, z_{bottom}, and z_{top} are the indices of the subsector's six boundaries. $u_{\max}$, $v_{\max}$, and $z_{\max}$ are the maximum values of the longitude, latitude, and altitude indices in the TMA, and $v_{\min}(u_{\mathrm{left}}, u_{\mathrm{right}})$ and $v_{\max}(u_{\mathrm{left}}, u_{\mathrm{right}})$ are the corresponding front and back boundaries within the range $(u_{\mathrm{left}}, u_{\mathrm{right}})$. Therefore, any subsector can be represented as all cells within the six boundaries.

$$S_{k,g} = \bigcup_{u=u_{\mathrm{left}}, v=v_{\mathrm{back}}, z=z_{\mathrm{bottom}}}^{u_{\mathrm{right}}, v_{\mathrm{front}}, z_{\mathrm{top}}} L\left(P'\right)_{\mathrm{uvz}}. \tag{12}$$

The problem of functional sectorization is transformed into the problem of finding $\sum_{k=1}^{K} s_k$ six tuples.

4.2. Optimization Model for Functional Sectorization

4.2.1. New Objective Function. The difference in the objective function is the most fundamental difference between functional and traditional sectorization. Traditional sectorization aims at optimizing the workload of ATC, which consists of two parts: balancing the workload between different sectors and minimizing the total coordination workload of all sectors. Many studies have demonstrated that these two objective functions contain intrinsic conflicts [20, 21, 25], while the functional consistency between the generated sector and the traffic flow, i.e., $J_{\mathrm{func-consis}}$, is offered as a novel optimization object in this paper. From the perspective of ATC, this object allows them to establish situational awareness and lessen the sector's safety hazards. From the pilot's perspective, this object eliminates the need to travel through different sectors, simplifying operational operations.

The functional consistency between the airspace sectors and air traffic flows, i.e., $J_{\mathrm{func-consis}}$, should be as large as possible, and this means that, for the airspace cells set with function k, the allocated sector S_k should cover the elements in the set as much as possible.

$$\mathrm{Obj}_{J(R)} = \max\left(\sum_{L\left(P'\right)_{\mathrm{uvz}} \in R} J_{\mathrm{func_{consis}}}\left(L\left(P'\right)_{\mathrm{uvz}}\right)\right), \tag{13}$$

where $J_{\mathrm{func\_consis}}(L(P')_{\mathrm{uvz}})$ is defined as follows:

$$J_{\mathrm{func-consis}}\left(L\left(P'\right)_{\mathrm{uvz}}\right) = \begin{cases} 1, \text{if } F\left(L\left(P'\right)_{\mathrm{uvz}}, k\right) == 1, \wedge \overset{\text{airspace cell allocated to sector } S_k}{L\left(P'\right)_{\mathrm{uvz}}} \in S_k, \\ \quad \text{if } F\left(L\left(P'\right)_{\mathrm{uvz}}, k\right) == 1, \wedge L\left(P'\right)_{\mathrm{uvz}} \notin S_k, \\ 0, \\ \quad \vee F\left(L\left(P'\right)_{\mathrm{uvz}}, k\right) == 0, \wedge L\left(P'\right)_{\mathrm{uvz}} \in S_k. \end{cases} \tag{14}$$

According to Equation (10), we can know that the function of the airspace cell is determined by the functions of

trajectories passing through the cell. Therefore, Equation (14) describes that the value of the objective function $J_{\text{func-consis}}(L(P')_{\text{uvz}})$ depends on whether airspace cell with function k is allocated to the corresponding sector S_k, which essentially reflects the consistency between the generated sector and the function of the traffic flow. If the function of the generated sector is more consistent with the function of the traffic flow in the sector, the larger the objective function will be.

4.2.2. Constraints. In the process of sectorization, in order to ensure the practicality of the scheme, various constraints need to be considered, which are introduced and formulated as follows.

(1) Right Prism Constraint. The sector is, without a doubt, a three-dimensional space scope. However, because the radar screen can only display a planar projection of the sector in the actual operation, the sector must be created in the shape of a right prism, as illustrated in Figure 6. The sector is represented by six tuples in this paper; therefore, it meets the right prism restriction naturally.

(2) Uniqueness Constraint. A sector can only be assigned to one single controller to avoid confusion and operational errors, so it is necessary to ensure that each airspace cell can only be assigned to one sector:

$$L\left(P'\right)_{\text{uvz}} \in S_{k,g} \Rightarrow L\left(P'\right)_{\text{uvz}} \notin \left(R \setminus S_{k,g}\right). \tag{15}$$

And it is represented in a six-tuple form as

$$\begin{aligned}&\left(\left(u_{\text{left}}, u_{\text{right}}\right)_{S_{k,g}} \cap \left(u_{\text{left}}, u_{\text{right}}\right)_{S_{i,j}} = \varnothing\right)\\ &\vee\left(\left(v_{\text{back}}, v_{\text{front}}\right)_{S_{k,g}} \cap \left(v_{\text{back}}, v_{\text{front}}\right)_{S_{i,j}} = \varnothing\right)\\ &\vee\left(\left(z_{\text{bottom}}, z_{top}\right)_{S_{k,g}} \cap \left(z_{\text{bottom}}, z_{top}\right)_{S_{i,j}} = \varnothing\right), (i \neq k \vee j \neq g).\end{aligned} \tag{16}$$

(3) Connectivity Constraint. The sector should be a closed space. In this paper, any subsector must contain all cells in the right prism defined by the six tuples and satisfy the connectivity internally. However, connectivity constraints should also be satisfied between subsectors, as expressed by the following equation:

$$\begin{aligned}&u_{\text{left}}\left(S_{k,g+1}\right) = u_{\text{right}}\left(S_{k,g}\right) + 1,\\ &\left(\left(v_{\text{back}}, v_{\text{front}}\right)_{S_{k,g}} \cap \left(v_{\text{back}}, v_{\text{front}}\right)_{S_{k,g+1}} \neq \varnothing\right)\\ &\vee\left(\left(z_{\text{bottom}}, z_{\text{top}}\right)_{S_{k,g}} \cap \left(z_{\text{bottom}}, z_{\text{top}}\right)_{S_{k,g+1}} \neq \varnothing\right).\end{aligned} \tag{17}$$

(4) Repeated Handover Constraint. Sector convexity constraint is often set in current research to avoid repeated handover of the same aircraft, as shown in Figure 7. However, the functional sector covers the mainstream trajectory and satisfies the repeated handover constraint naturally.

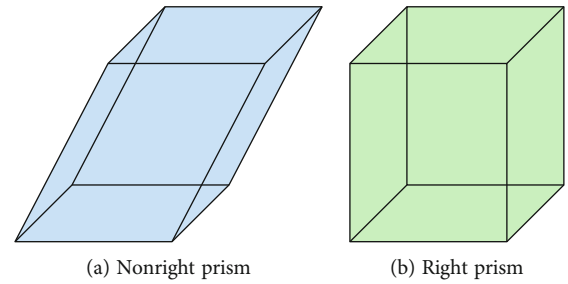

Figure 6: Right prism constraint.

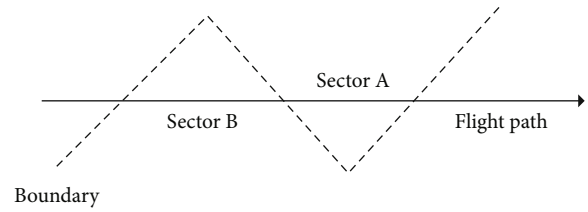

Figure 7: Repeated handover constraint.

(5) Integrity Constraint. According to the objective function, we can find that the blank cells do not affect the objective function. However, all the airspace resources in the TMA should be utilized as much as possible, i.e., all the airspace cells should be assigned to a certain type of functional sector. Therefore, the algorithm design needs to consider how to allocate the blank cells and ensure that each sector after allocation still satisfies the above four constraints.

5. Design of Functional Sectorization Algorithm

Since it is difficult to generate solutions satisfying all constraints directly, the solutions satisfying the constraints are gradually generated, which are realized by the following three rules, respectively.

5.1. Initial Generation Rule. The initial generation rule is used to randomly generate the initial solution of the functional sector by searching $\sum_{k=1}^{K} s_k$ six tuples. The initial solution generated by this rule satisfies the connectivity constraint by the following steps.

Step 1. Get the left and right boundaries of the cells passed through by the kth cluster of trajectories as the left and right boundaries of the horizontal range of the functional sector S_k. Randomly generate numbers $u1$ and $u2$ within this range to divide the sector into three consecutive subsectors $S_{k,1}$, $S_{k,2}$, and $S_{k,3}$. The left and right boundaries of the three subsectors are $(u_{\text{left}}, u1)$, $(u1+1, u2)$, and $(u2+1, u_{\text{right}})$, respectively. If $u1 == u_{\text{left}}$, $u1 == u2$, or $u2 == u_{\text{right}}$, the corresponding subsector does not exist.

Step 2. Within the left and right boundaries of each subsector, get the horizontal front and back boundaries of the cells passed through by the kth cluster of trajectories as the front

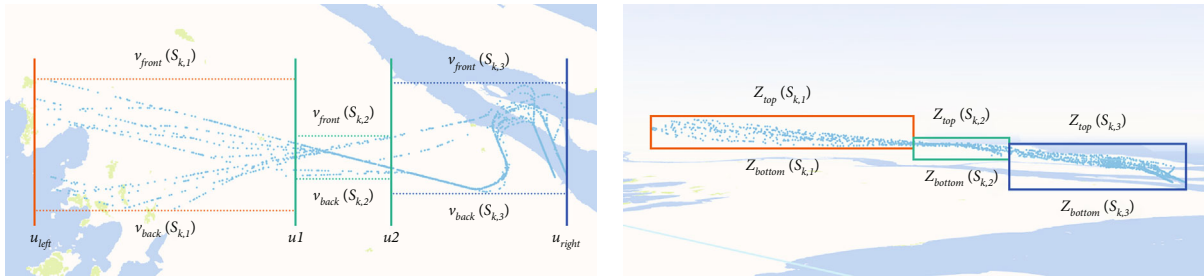

(a) Horizontal range (b) Vertical range

Figure 8: Initial generation process of the functional sector.

Input: All Functional Sectors and *OrderS*
Output: Adjusted Sectors
1: **for** i **in** *OrderS* **do**
2: $S_k \Leftarrow All\ Sectors(i)$
3: **for** j **in** 1,2…$i-1$ **do**
4: $S_j \Leftarrow All\ Sectors(j)$
5: **if** S_k intersect with S_j **then**
6: $z_{ava}(S_{k,g}) \Leftarrow (z_{bottom}, z_{top})_{S_{k,g}} - (z_{bottom}, z_{top})_{S_{i,j}}$
7: **end if**
8: find all consecutive height intervals z_{ava}
9: **if** z_{ava} exists **then**
10: find the height interval $z_{ava}(S_{k,1})_p$ with longest interval length
11: $(z_{bottom}, z_{top})_{S_k} \Leftarrow z_{ava}(S_{k,1})_p$
12: **else**
13: extend available vertical range to $(1, z_{\max})$
14: **go to** find all consecutive height intervals z_{ava}
15: **end if**

Algorithm 1: Judgment and adjustment

and back boundaries of each subsector $(v_{\text{back}}, v_{\text{front}})$ and the bottom and top $(z_{\text{bottom}}, z_{\text{top}})$ as a vertical range. The six tuples of the initial solution for the functional sector S_k are as follows:

$$\begin{aligned} S_{k,1} &= \{u_{\text{left}}, u1, v_{\text{back}}(S_{k,1}), v_{\text{front}}(S_{k,1}), z_{\text{bottom}}(S_{k,1}), z_{\text{top}}(S_{k,1})\}, \\ S_{k,2} &= \{u1+1, u2, v_{\text{back}}(S_{k,2}), v_{\text{front}}(S_{k,2}), z_{\text{bottom}}(S_{k,2}), z_{\text{top}}(S_{k,2})\}, \\ S_{k,3} &= \{u2+1, u_{\text{right}}, v_{\text{back}}(S_{k,3}), v_{\text{front}}(S_{k,3}), z_{\text{bottom}}(S_{k,3}), z_{\text{top}}(S_{k,3})\}. \end{aligned} \tag{18}$$

Step 3. Repeat the above steps K times to generate initial solutions for each functional sector. Figure 8 shows the initial generation process of the functional sector according to one cluster of trajectories.

5.2. Judgment and Adjustment Rule. The uniqueness constraint requires no overlap in the spatial extent between different sectors. Therefore, it is necessary to judge and adjust the overlap of the initial solution. The judgment rule is first introduced below. Suppose that the sectorization order is Order$S$ = $\{S_{i_1}, S_{i_2}, \cdots, S_{i_K}\}$, the former sector is S_k, and the latter sector is S_i. The process of judgment and adjustment is shown in Algorithm 1.

5.2.1. Judgment Rule. If two sectors overlap, it means that the subsectors of the two sectors also overlap, which is represented by a symbol $\otimes$. The way to judge the subsector overlap can be expressed as

$$\begin{aligned} S_{k,g} \otimes S_{i,g} = &\left((u_{\text{left}}, u_{\text{right}})_{S_{k,g}} \cap (u_{\text{left}}, u_{\text{right}})_{S_{i,j}} \neq \varnothing\right) \wedge, \\ &\left((v_{\text{back}}, v_{\text{front}})_{S_{k,g}} \cap (v_{\text{back}}, v_{\text{front}})_{S_{i,j}} \neq \varnothing\right) \wedge, \\ &\left((z_{\text{bottom}}, z_{\text{top}})_{S_{k,g}} \cap (z_{\text{bottom}}, z_{\text{top}})_{S_{i,j}} \neq \varnothing\right). \end{aligned} \tag{19}$$

Therefore, if the two sectors overlap, it can be expressed as:

$$S_k \otimes S_i = \bigcup_{g=1,j=1}^{n_k,n_i} \left(S_{k,g} \otimes S_{i,j}\right). \tag{20}$$

5.2.2. Adjustment Principle. The adjustment of the initial solution mainly includes the adjustment of the sector generation

Input: Energy Objective $J()$
Output: the optimal solution $s_{optimal}$
Set initial temperature $T_0 \longleftarrow T_{\min}$
generate an initial solution $s_0 \longleftarrow Initial\ generation\ rule()$
initiate control parameters $iterMax$, $T_{\max}$, $coolrate$
$T \longleftarrow T_{\max}$
calculate initial objective $J(s_0)$, set $J(s_{optimal}) \longleftarrow J(s_0)$
∗the stopping criterion
while $T > T_{\min}$ **do**
  $s_{new} \longleftarrow transform(s)$
∗neighbor selecting
    calculate $E(s_{new})$
    calculate the acceptance probability $P(E(s), E(s_{new}), T)$
    if $P(E(s), E(s_{new}), T) \geq random(0, 1)$ **then**
      move to the new solution: $s \longleftarrow s_{new}$
    end if
    if $E(s_{new}) > E(s_{optimal})$ **then**
      $s_{optimal} \longleftarrow s_{new}$
    end if
$T \longleftarrow T * coolrate$
Transform Function():
    input: solution s
    output: new neighbor solution s_{new}
    for each sector **in** s **do**
      randomly adjust vertical range and horizontal range within (-3,3)
    check the legality of new solution s_{new}
    if legal **then**
      return s_{new}
    else
      apply adjust rules to s_{new}

Algorithm 2: Simulated annealing.

order and the spatial range of each sector. Based on the visual analysis of the trajectories, the following adjustment principles are proposed:

(1) Since there are often horizontal crossings between the trajectories with different functions, they are separated from each other vertically to ensure sufficient safety separation. Therefore, for the overlap of different sectors, priority is also given to adjusting the vertical range of the sectors to make them separated in height

(2) When selecting an adjustment target, S_k and S_i are selected to adjust, and the priority is given to reassigning a sector whose overlapping portion accounts for a larger proportion of the entire sector

(3) Considering that functional sectors are generated in a specific order, the later the sector is generated, the smaller the space that can be adjusted. The probability of making adjustments to the former sector S_k should be lower than that of the latter sector S_i.

5.2.3. Adjustment Rule. According to the definition of overlap and adjustment principles, if two subsectors $S_{k,g}$ and $S_{i,j}$ overlap, their available vertical range will be reduced, which can be calculated by

$$\begin{aligned} z_{\text{ava}}\left(S_{k,g}\right) &= \left(z_{\text{bottom}}, z_{\text{top}}\right)_{S_{k,g}} - \left(z_{\text{bottom}}, z_{\text{top}}\right)_{S_{i,j}}, \\ z_{\text{ava}}\left(S_{i,j}\right) &= \left(z_{\text{bottom}}, z_{\text{top}}\right)_{S_{i,j}} - \left(z_{\text{bottom}}, z_{\text{top}}\right)_{S_{k,g}}. \end{aligned} \tag{21}$$

Due to the possibility of nesting, the available vertical range is divided into multiple intervals. The sector to be adjusted is selected by probability, assuming that it is S_k. According to the reduced available range, the specific adjustment algorithm is as follows:

Step 1. Iterate over available vertical ranges $z_{\text{ava}}(S_{k,1}), z_{\text{ava}}(S_{k,2}), \cdots, z_{\text{ava}}(S_{k,s_k})$, and find all consecutive height intervals:

$$\begin{aligned} &\left(z_{\text{ava}}(S_{k,1})_1, z_{\text{ava}}(S_{k,2})_1, \cdots, z_{\text{ava}}\left(S_{k,s_k}\right)_1\right), \\ &\left(z_{\text{ava}}(S_{k,1})_2, z_{\text{ava}}(S_{k,2})_2, \cdots, z_{\text{ava}}\left(S_{k,s_k}\right)_2\right), \\ &\left(z_{\text{ava}}(S_{k,1})_p, z_{\text{ava}}(S_{k,2})_p, \cdots, z_{\text{ava}}\left(S_{k,s_k}\right)_p\right), \end{aligned} \tag{22}$$

where $z_{\text{ava}}(S_{k,1})_p$ is an available height interval, and there are p groups of consecutive height intervals.

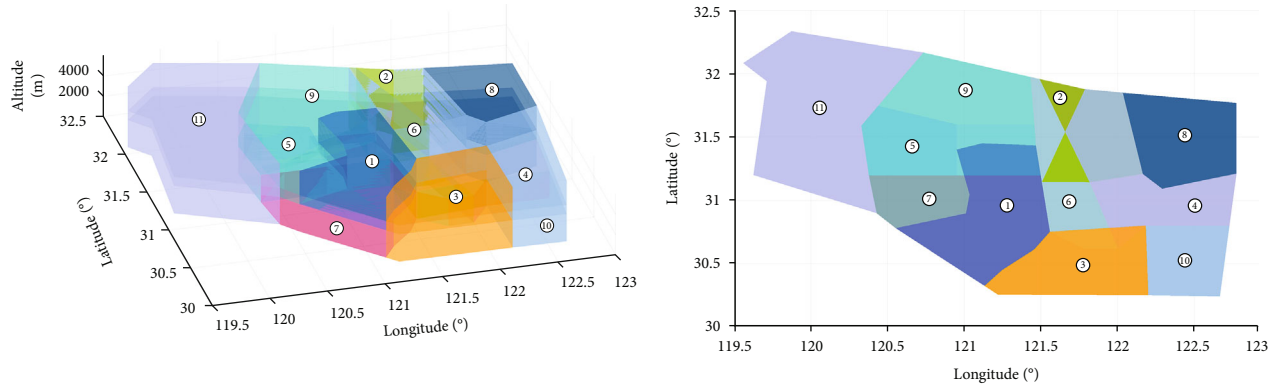

(a) 3D view (b) 2D view

Figure 9: Current sectors of the Shanghai TMA.

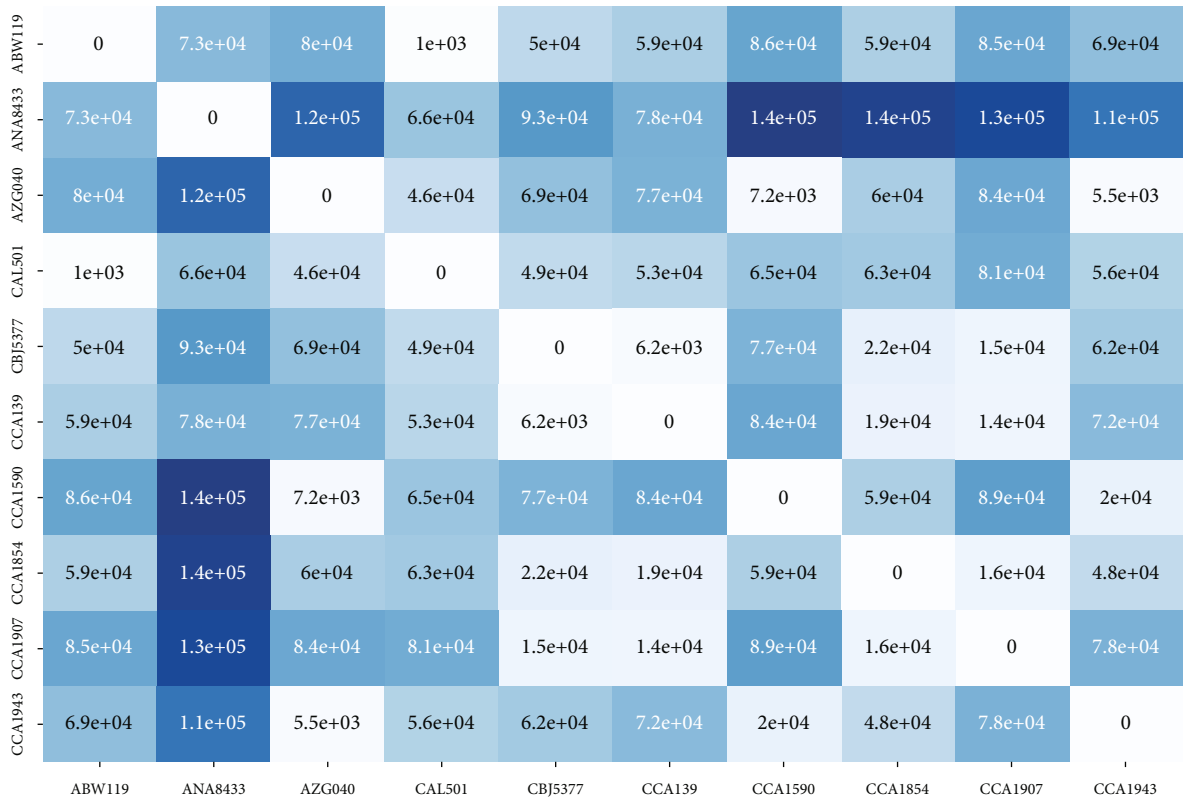

Figure 10: Partial distance matrix between different trajectories.

Step 2. If consecutive height intervals can be found, then the total lengths of p groups of height intervals are calculated, and the intervals with the longest total length are taken as the new vertical range of the sector S_k.

Step 3. If a set of consecutive height intervals cannot be found, i.e., $p = 0$, the former sector S_k cannot be adjusted, and the latter sector S_i is readjusted. Extend the available vertical range to $(1, z_{\max})$ and refind consecutive height intervals.

The above algorithm adjusts the vertical range for the two sectors with overlap, and the connectivity constraint is satisfied in the adjustment process.

5.3. Gap-Filling Rule. After completing the assignment of the six tuples for each functional sector, there are many blank cells left. It is necessary to make all the blank cells assigned to the functional sector for the integrity constraint. The steps are as follows:

Step 1. Traverse the unassigned blank cells, and find a cuboid group of blank cells.

Step 2. Find all functional sectors adjacent to the cell group, and traverse each functional sector.

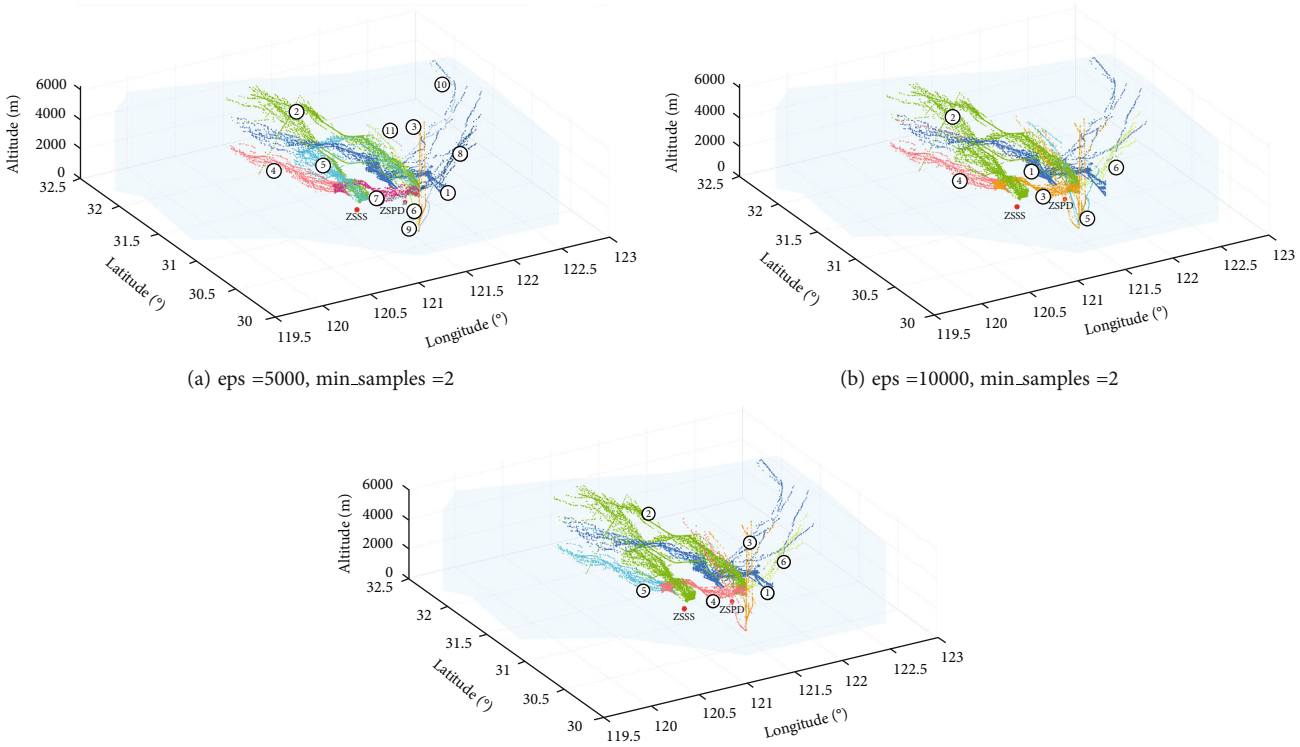

(a) eps =5000, min_samples =2

(b) eps =10000, min_samples =2

(c) eps =10000, min_samples =5

Figure 11: Comparison of trajectory clustering results under different parameter settings.

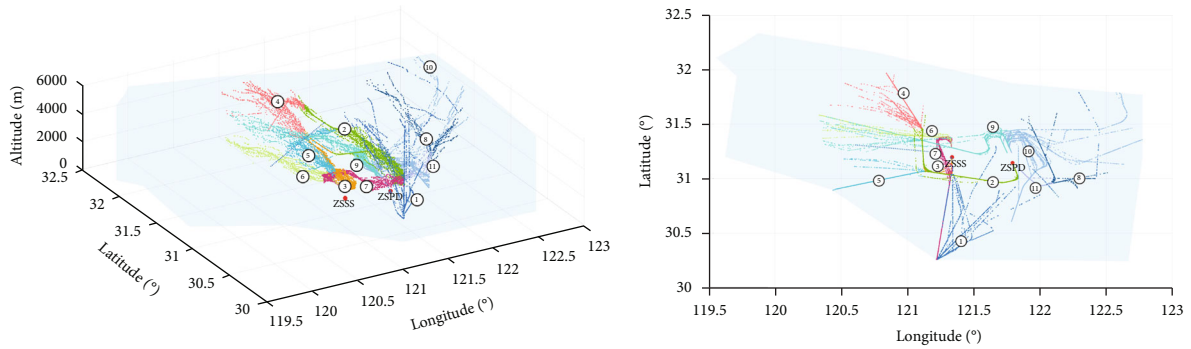

(a) 3D view

(b) 2D view

Figure 12: 11 clusters of trajectories.

Step 3. For each function sector, calculate the minimum cuboid surrounding it and the ratio of the number of functional sector cells to the number of minimum cuboid cells.

Step 4. Try to assign the blank cuboid group to each sector and repeat Step 3.

Step 5. Choose the sector with the largest ratio increase to receive the blank cell group finally.

Step 6. Repeat the above steps until all blank cells have been allocated.

Considering that the rule has little effect on the objective function, the above allocation process is only for the regularity of the sector shape. It is not performed every time during the optimization process but is performed after the optimal solution is solved.

The computational complexity of the above rules is low, which reduces the computational burden for further optimization of the solution.

5.4. Optimization Process. The result of sectorization is affected by the horizontal and vertical ranges and the order of sectorization, so the above factors are selected as variables. The solution for a sector is represented by a list of length 7, where the left and right boundaries are fixed, so the first two

Table 1: Comparison of spatial elements with different side lengths.

Edge length (km)	The number of cells	The number of cells passed through by trajectories	The number of cells passed through by multiple clusters of trajectories
2.86	54140	2095	74
3.82	31000	1612	64
4.77	19900	1315	64

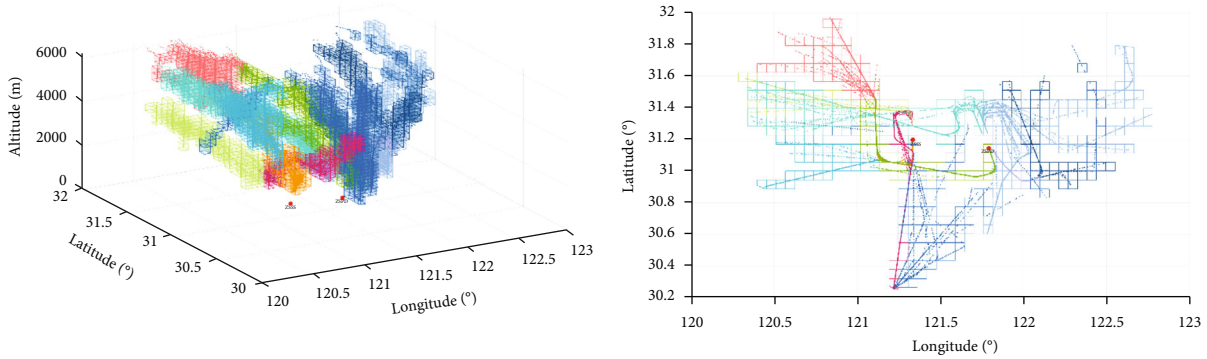

(a) 3D view (b) 2D view

Figure 13: The functions of airspace cells in the Shanghai TMA.

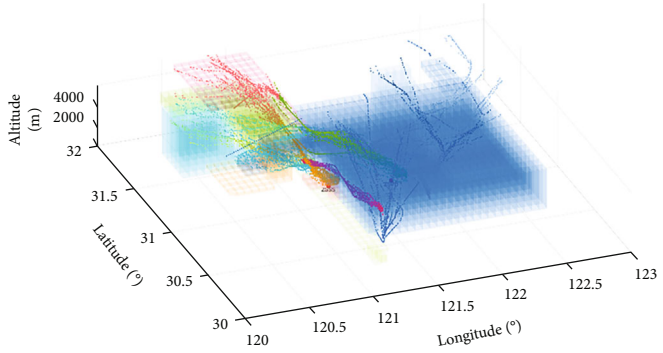

Figure 14: Feasible solution of functional sectors.

variables are the horizontal partition positions of the subsectors alternatively, and the rest are the front and back boundaries and the top and bottom of each subsector. The resulting solution for all sectors is expressed as

$$\mathrm{Sol}(R) = \begin{bmatrix} \mathrm{Sol}_1 \\ \cdots \\ \mathrm{Sol}_K \\ \mathrm{Order}S \end{bmatrix}. \tag{23}$$

The problem of the functional sectorization belongs to the large-scale stochastic optimization problem, so this paper uses a simulated annealing algorithm to solve the functional sectorization problem. The simulated annealing algorithm has the advantages of high operational efficiency, fewer initial condition constraints, and can break through the local and avoid falling into the optimal local solution [43]. The specific flow of the optimization process is given in Algorithm 2.

6. Experimental Evaluation and Results

6.1. Experiment Setup: Data Preparation. Shanghai is China's busiest metropolis, serving as the country's commercial center and the pioneer city of the civil aviation industry. The Shanghai TMA is 230 kilometers long from east to west and 180 kilometers broad from north to south, with an altitude of 6,000 meters. The primary responsibility of the Shanghai TMA is to provide air traffic control services for the arrival and departure flights of Shanghai Hongqiao International Airport (ZSSS) and Shanghai Pudong International Airport (ZSPD), as well as overflights from other airports within the jurisdiction and surrounding airports. Currently, the Shanghai TMA is divided into 11 sectors, as shown in Figure 9.

In terms of traffic flow data, 19230 points belonging to 167 trajectories in the Shanghai TMA from 9:00 to 10:00 on June 15, 2021, were selected.

6.2. Experimental Details: Functional Sectorization Process. The similarity matrix for point-by-point comparison was

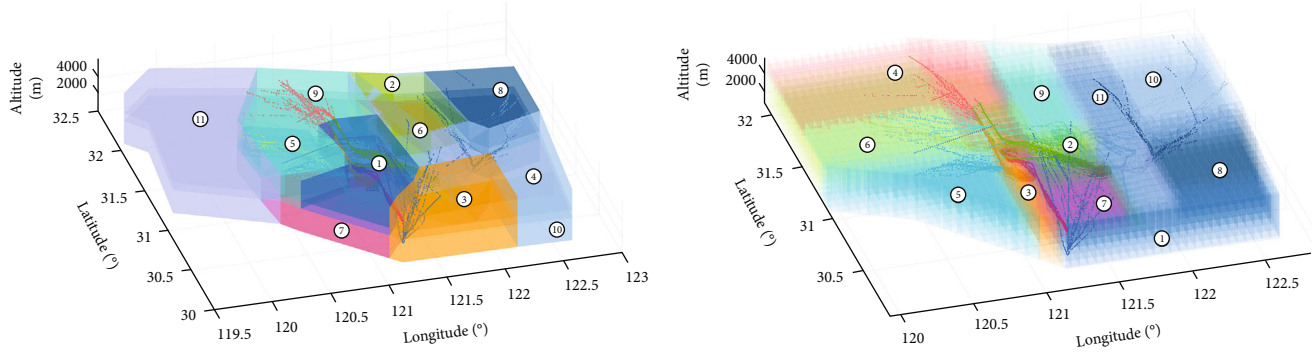

(a) Current sectors (b) Functional sectors

FIGURE 15: Before-and-after results: (a) without (b) with the proposed functional sectorization method.

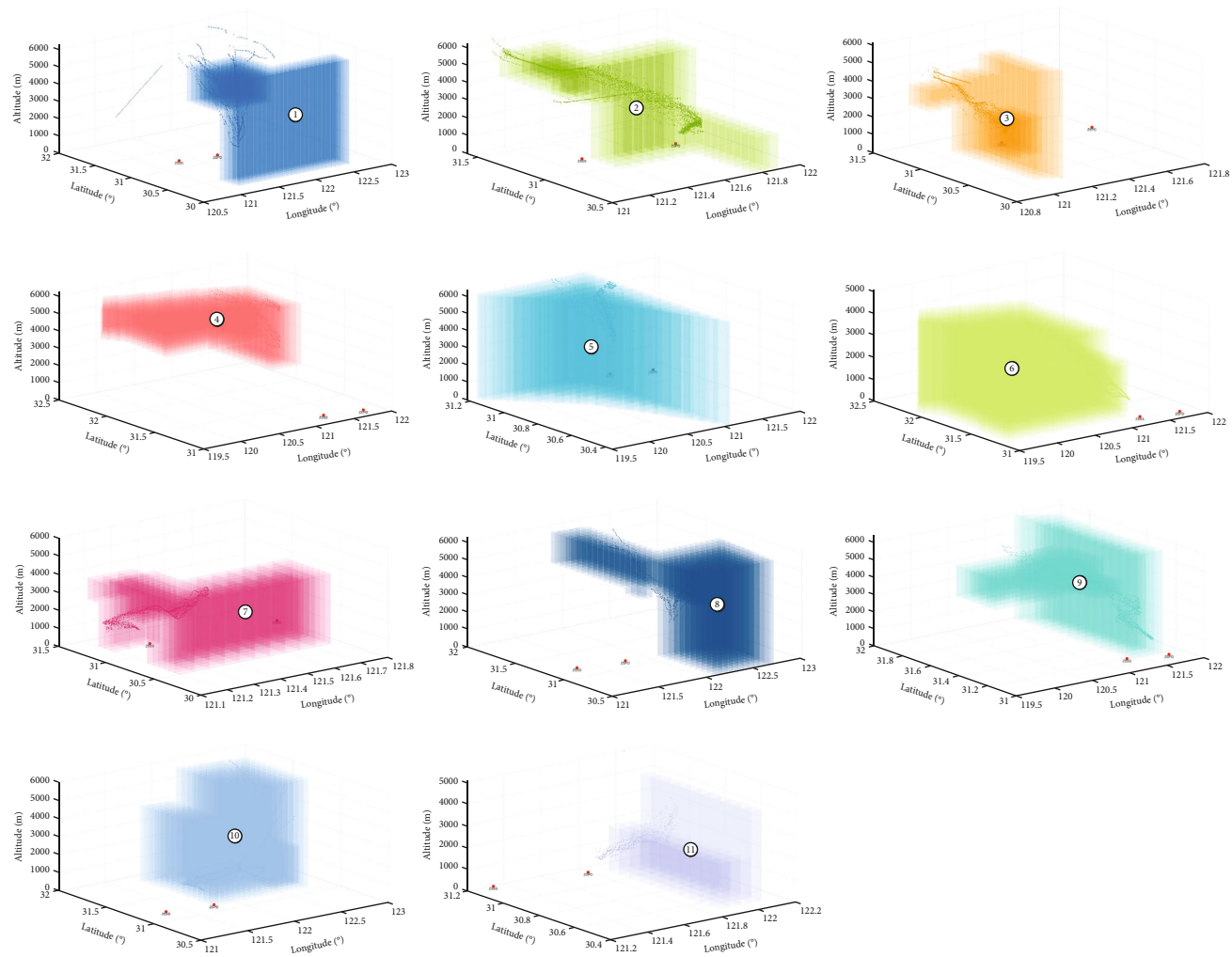

FIGURE 16: Details of each functional sector and the trajectories passing through it.

established based on the above trajectory data during the peak hour, and a large number of trajectories, partial results, are shown in Figure 10.

The distances between the trajectories vary widely, encompassing numerous orders of magnitude, suggesting that the distance computation method based on the point-by-point comparison used in this work can measure the similarity between trajectories and separate distant trajectories. The DBSCAN algorithm was used to do clustering based on this distance matrix, and the two primary parameters of the DBSCAN algorithm were changed. In Figure 11, the clustering results of the trajectories are given for various parameter values.

The gray trajectory points are noise, and the rest of the different colors indicate different clusters of trajectories.

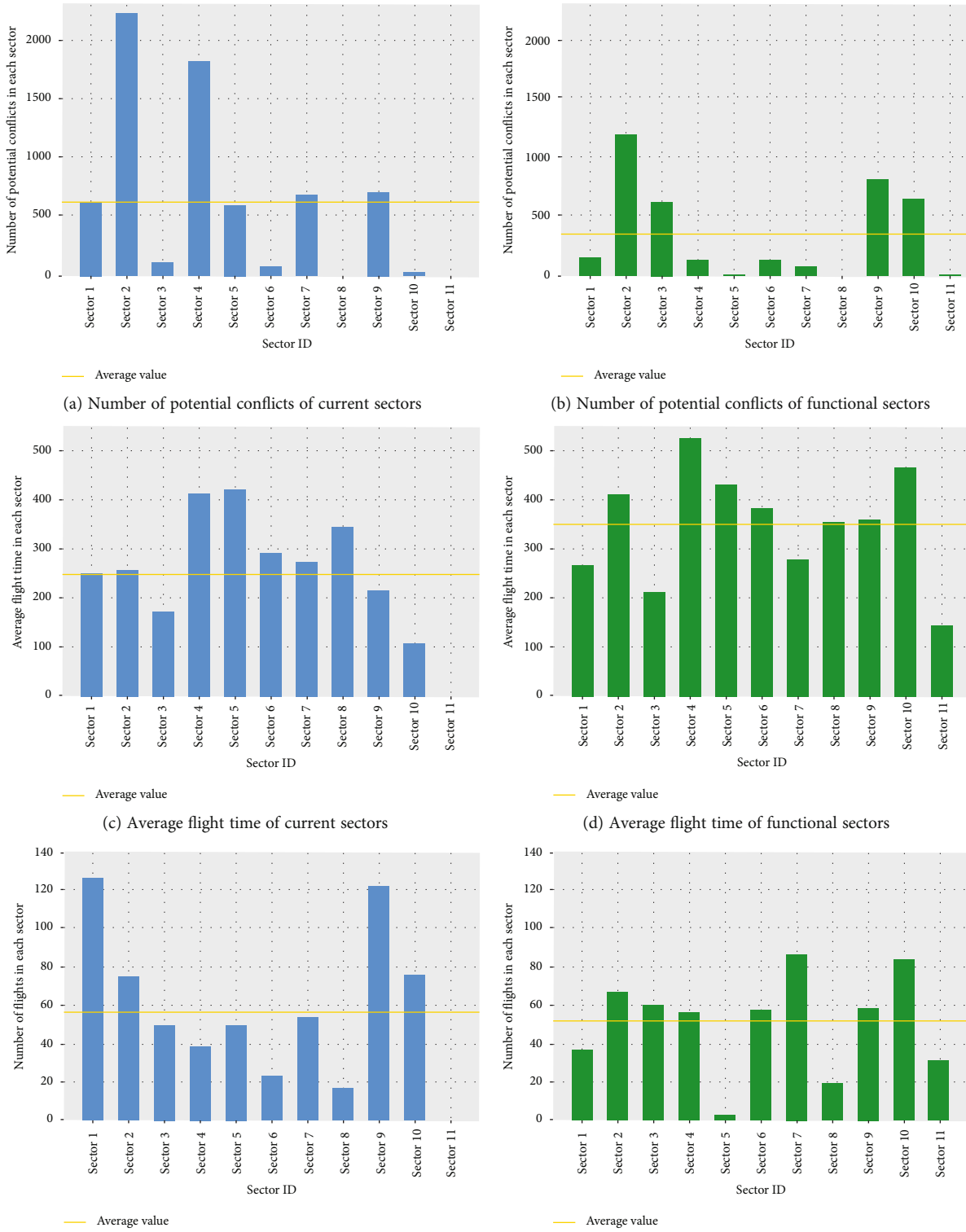

(a) Number of potential conflicts of current sectors

(b) Number of potential conflicts of functional sectors

(c) Average flight time of current sectors

(d) Average flight time of functional sectors

(e) Traffic density of current sectors

(f) Traffic density of functional sectors

Figure 17: Comparison of different indicators between the current sector and functional sector.

Comparing the above results, we can find that different parameter settings have a great impact on the clustering results of trajectories. There are 11 clusters of trajectories in Figure 11(a), while in Figures 11(b) and 11 (c), there are 6 clusters, indicating that a larger eps leads to fewer clustering results, and trajectories are more likely to be clustered into one cluster. In addition, some of the overflight trajectories were misclassified as noise points with the increase of

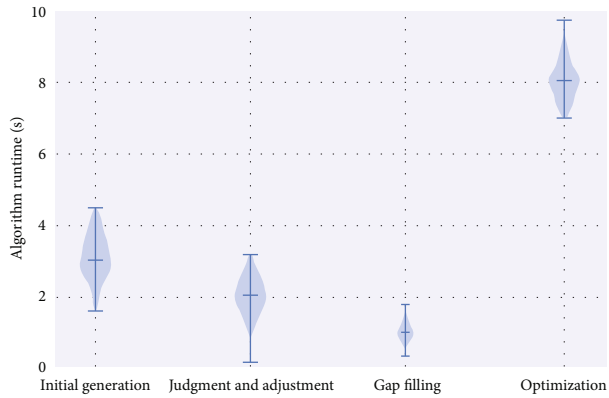

Figure 18: The running time of each stage of the functional sectorization algorithm.

min_samples. Because the overflight trajectories are far away from the others, so there are not enough trajectories nearby to meet the requirements when min_samples is greater.

By tweaking the parameters several times, the parameters were determined as eps = 10000 and min_samples = 2. Then, combined with the flight procedures, we finally have 11 clusters of trajectories, as shown in Figure 12.

In Figure 12, the different functional trajectories are well separated. The 1st cluster of trajectories are overflights, the 2nd cluster of trajectories are initial departures from ZSPD to the northwest, the 3rd cluster of trajectories are initial departures from ZSSS to the northwest, the 4th cluster of trajectories are departures from ZSPD and ZSSS to the northwest, the 5th cluster of trajectories are departures from ZSPD to the west, the 6th cluster of trajectories are arrivals from the west to ZSSS, the 7th cluster of trajectories are arrivals from the south to ZSSS, the 8th cluster of trajectories are departures from ZSPD to the east, the 9th cluster of trajectories is arrivals from the west to ZSPD, the 10th cluster of trajectories are arrivals to ZSPD, and the 11th cluster of trajectories are initial departures from ZSPD to the east.

Then, the Shanghai TMA discretization was performed. There were various parameters to set during the airspace discretization process, one of which was the center point, which had no effect on the result and was set to ZSSS. The TMA was divided into 20 layers vertically, with each layer's altitude set at 300 m according to the standard height of flight level. The horizontal edge length was undoubtedly the most important parameter; the edge length directly affected cell size; too large cells result in one cell covering many trajectory points, resulting in inaccurate segmentation; too small cells result in a sharp increase in the number of cells, resulting in high calculation costs and poor practicality. As a result, the edge length parameter had to be adjusted to create a better balance between accuracy and computational cost. Table 1 displays the results of the change, and the edge length was finally fixed at 3.82 km.

Once the discretization of the airspace was completed, the function of each cell can be determined. If one cell was passed through by multiple clusters of trajectories, it accordingly had multiple functions. The calculation results of cells function are shown in Figure 13. As there are many blank cells, it is not easy to observe if all of them are displayed, so only the functional cells passed through by the trajectory, i.e., functional cells, are shown.

The Shanghai TMA was discretized into 31,000 cells, of which 1612 are functional cells and the remaining are blank. The blank cells only play a role in the final stage of the gap-filling rule of the algorithm, and 1612 functional cells are closely related to the objective function. The object of the functional sectorization assignment is to assign as many functional cells as possible to the corresponding functional sectors, i.e., to match the function of the sector with that of the trajectories passing through the sector.

Next, feasible solutions are generated by the algorithm in Section 5. After 1000 random executions of the algorithm, the resulting feasible solution is shown in Figure 14 with an objective function of 256.

It can be seen that the randomly generated feasible solution has been able to satisfy the uniqueness constraint, connectivity constraint, and right prism constraint, which proves the effectiveness of the algorithm in this paper. However, it is not accurate enough in terms of horizontal and vertical ranges, such as overflight airspace, which should have allocated fewer cells to meet the demand of other functional sectors. Therefore, the objective function of the feasible solution is not satisfactory for it can only assign 15.88% of the functional cells to the corresponding sectors, while the function of the remaining 84.12% of cells does not match the function of the sector.

After that, optimization by a simulated annealing algorithm is required to find a better solution for the objective function. From multiple perspectives such as convergence speed and algorithm execution efficiency, we set the simulated annealing algorithm parameters as the initial temperature $T_{\max}$, cooling rate delta = 0.95, number of iterations within each temperature iterNum = 100, and minimum termination temperature $T_{\min}$. After optimization, the objective function is 1503; this solution can allocate 93.24% of the functional cells to the corresponding sectors, which are the optimal functional sectors. Due to constraints, particularly the right prism constraint, the remaining 6.76% of functional cells could not be assigned to the appropriate sectors.

Figure 15 shows the comparison of current sectors and functional sectors in general, and Figure 16 shows the details of each functional sector and the trajectories passing through it.

It can be seen that compared with simultaneously existing different clusters of traffic flows in the same current sector, the different clusters of traffic flows are well separated and recognized in functional sectors. That is, each functional sector accurately covers one cluster of trajectories, and thus, the validity of the algorithm is verified. The first functional sector that corresponds to the overflight trajectories appears to be poorly designed, which indicates that it cannot entirely cover the overflight trajectories. This is due to the fact that the overflight trajectories are dispersed. More airspace must be provided to the overflight trajectories if it is to be entirely covered. However, the number of overflight trajectories is minimal, and allocating more airspace to them will inevitably consume the viable solution space of the equivalent sectors of other mainstream trajectories, resulting in a loss of the objective function.

Table 2: Comparison of operational benefits between the current sector and functional sector.

	Number of potential conflicts	Average sector flight time (s)	Traffic density variance	Average number of traversed sectors
Current sector	6890	250.10	38.16	2.78
Functional sector	3797	346.63	24.47	1.67
Percentage of improvement (%)	44.89	38.60	35.8	39.92

6.3. Results and Discussion: Performance Evaluation. Although there has been considerable research on the performance evaluation of the airspace system, there has been few research on that of sectorization, especially on the sectorization in the TMA. To further evaluate the performance of functional sectors, this study selected the following five indicators from two aspects of safety and efficiency:

(1) *Number of Potential Conflicts in Each Sector*. The potential conflicts are called crossing points in literature 21, which measures the safety level of the sectorization. However, the time interval is defined as 300 s in the literature 21, which is divorced from the current operation reality. After several experiments and combining the experience of ATCs, we improved the definition in the literature 21 as follows

$$\begin{aligned} & d\left(p_m\left(\ln g_{p_m}, \mathrm{lat}_{p_m}\right), q_n\left(\ln g_{q_n}, \mathrm{lat}_{q_n}\right)\right) \\ & \quad \le 10\mathrm{km} \vee \left|p_m\left(\mathrm{alt}_{p_m}\right) - q_n\left(\mathrm{alt}_{q_n}\right)\right| \\ & \quad \le 300\mathrm{m} \vee \left|\mathrm{time}_{p_m} - \mathrm{time}_{q_n}\right| \le 60\mathrm{s}. \end{aligned} \tag{24}$$

where p_m and q_n are the positions of aircraft p and q at the time time_{p_m} and time_{q_n}.

(2) *Average Sector Flight Time*. The average sector flight time is the average flight time of flights in each sector. The long sector flight time means the alignment between sectors and traffic flows and the small traffic cuts by sector [20]. Furthermore, research indicates that the capacity of each sector is directly related to the average sector, and sectors with longer average flight times will have higher capacity [17]

(3) *Traffic Density Variance*. The traffic density variance is the variance of flights in each sector within a given time period. Traffic density is one of the indicators that measure the monitoring workload of ATC, and sectors with high traffic density make ATC have a high monitoring workload. Therefore, traffic density variance reflects the fairness of the monitoring workload of ATCs in different sectors, which is the main optimization object of traditional sectorization [25, 26]

(4) *Average Number of Traversed Sectors*. The average number of traversed sectors is the average number of sectors that each flight traverses, which measures the coordination workload of ATC. A smaller average number of traversed sectors means fewer handovers and coordination, which is also an essential optimization object of traditional sectorization [25, 26]

(5) *Algorithm Runtime*. Runtime is an important performance metric for algorithms [44]. By calculating the general runtime of the algorithm from multiple experiments and observing the distribution of running time in each phase, the efficiency of the functional sectorization algorithm can be reflected

Overall, the number of potential conflicts in each sector indicates the safety level of sectorization; the average sector flight time indicates the sector capacity; the traffic density variance and the average number of traversed sectors indicate the monitoring and coordination workload of ATC. Figure 17 shows the number of potential conflicts, flight time, and traffic density of each sector in current sectors and functional sectors.

From Figure 17, we can see that almost each sector has improved in terms of the three metrics. This is because the functional sector can cover the mainstream of a traffic flow so that most flights in the TMA only need to pass through one sector, the average number of traversed sectors is reduced, and the flight time in each sector is increased, thus improving the coordination workload of ATC, while the balance of monitoring workload mainly depends on the uniform distribution of traffic flows with different functions in the TMA. In addition, traffic flows of different functions often have the risk of intersection conflicts, which requires the human intervention of controllers to resolve conflicts in time. Functional sectors can reduce the potential conflicts of aircraft within the sector by separating traffic flows of different functions, thus ensuring a reasonable allocation of airspace resources.

Figure 18 depicts the distribution of running times for each algorithmic phase after 100 runs. The functional sectorization algorithm runs for a total of around 14 s, with initial generation takes approximately 3 seconds, judgment and adjustment approximately 2 seconds, gap filling approximately 1 second, and optimization approximately 8 seconds.

The overall comparison between the current sectors and functional sectors is shown in Table 2 as follows. Compared with the current sector, the four indicators of the functional sector have all improved, among which the potential conflicts within the sector have been reduced by 44.89%, the average sector flight time has been increased by 38.60%,

the traffic density variance has been reduced by 35.8%, and the average number of traversed sectors has been reduced by 39.92%.

7. Conclusion

Based on the function of air traffic and airspace, this paper studies the problem of functional sectorization in the TMA. Firstly, the traffic flow functions are classified through the clustering of flight trajectories. Then, the TMA is discretized, and a framework of functional sectorization is established to generate sectors with specific functions, where a novel optimization object is proposed: the functional consistency between sectors and air traffic flows. After that, a corresponding algorithm is designed with an initial generation rule, judgment and adjustment rule, gap-filling rule, and optimization process to generate functional sectors. Finally, experimental evaluation based on the Shanghai TMA is performed. Experiments show that the proposed functional sectorization method can generate sectors where operating functions are consistent with traversed traffic flow functions. Moreover, the optimization goal of the functional consistency between sectors and air traffic flows can improve the safety level, increase the capacity of TMA, and optimize the workload of ATC. Specifically, compared with current sectors, potential conflicts within the functional sector have been reduced by 44.89%, the average sector flight time has been increased by 38.60%, the traffic density variance has been reduced by 35.8%, and the average number of traversed sectors has been reduced by 39.92%. In the future, we will extend the work by conducting sensitivity analysis under different operation situations (weather or military activities), as well as dynamic configurations of functional sectors according to the changes in air traffic.

Data Availability

The data used to support this research acritical are available from the corresponding author on request.

Conflicts of Interest

The authors declare no conflict of interest.

Acknowledgments

This research was funded by the National Natural Science Foundation of China, grant number U1933119. This research was also funded by the Foundation of Graduate Innovation Center in Nanjing University of Aeronautics and Astronautics, grant number xcxjh20210703.

References

[1] International Civil Aviation Organization, *2016-2030 Global Air Navigation Plan*, International Civil Aviation Organization, Montreal, Canada, 2016.

[2] H. Wang, Z. Song, R. Wen, and Y. Zhao, "Study on evolution characteristics of air traffic situation complexity based on complex network theory," *Aerospace Science and Technology*, vol. 58, pp. 518–528, 2016.

[3] Y. Xu, H. Zhang, Z. Liao, and L. Yang, "A dynamic air traffic model for analyzing relationship patterns of traffic flow parameters in terminal airspace," *Aerospace Science and Technology*, vol. 55, pp. 10–23, 2016.

[4] H. Hering, "Air traffic freeway system for Europe," Eurocontrol Experimental Centre, Cedex, France, 2005.

[5] International Civil Aviation Organization, *Procedures for Air Navigation Services-Aircraft Operations: Doc8168*, International Civil Aviation Organization, Montreal, Canada, 2018.

[6] International Civil Aviation Organization, *Manual on Airspace Planning Methodology for the Determination of Separation Minima: Doc9689-AN/953*, International Civil Aviation Organization, Montreal, Canada, 2018.

[7] International Civil Aviation Organization, *Air Traffic Services Planning Manual: Doc 9426-AN/924*, International Civil Aviation Organization, Montreal, Canada, 1984.

[8] X. Zou, P. Cheng, B. An, and J. Song, "Sectorization and configuration transition in airspace design," *Mathematical Problems in Engineering*, vol. 2016, Article ID 6048326, 21 pages, 2016.

[9] D. Delahaye, J.-M. Alliot, M. Schoenauer, and J.-L. Farges, "Genetic algorithms for partitioning air space," in *Proceedings of the Tenth Conference on Artificial Intelligence for Applications*, pp. 291–297, San Antonio, TX, USA, 1994.

[10] D. Delahaye, M. Schoenauer, and J. M. Alliot, "Airspace sectoring by evolutionary computation," in *1998 IEEE International Conference on Evolutionary Computation Proceedings. IEEE World Congress on Computational Intelligence (Cat. No.98TH8360)*, pp. 218–223, Anchorage, AK, USA, 1998.

[11] S. C. Han and M. Zhang, "The optimization method of the sector partition based on metamorphic Voronoi polygon," *Chinese Journal of Aeronautics*, vol. 17, no. 1, pp. 7–12, 2004.

[12] A. Yousefi and G. Donohue, "Temporal and spatial distribution of airspace complexity for air traffic controller workload-based sectorization," in *AIAA 4th Aviation Technology, Integration and Operations (ATIO) Forum*, Chicago, Illinois, 2004.

[13] A. Klein, "An efficient method for airspace analysis and partitioning based on equalized traffic mass," *Proceedings of the 6th USA/Europe Air Traffic Management R & D Seminar*, George Mason University, George, VA, USA, 2005.

[14] C. Brinton, J. Hinkey, and K. Leiden, "Airspace sectorization by dynamic density," in *9th AIAA Aviation Technology, Integration, and Operations Conference (ATIO)*, Head, South Carolina, 2009.

[15] M. Bloem and P. Gupta, "Configuring airspace sectors with approximate dynamic programming," *International Congress of the Aeronautical Sciences*, 2010.

[16] P. Jagare, P. Flener, and J. Pearson, "Airspace sectorisation using constraint-based local search," in *ATM 2013; 2013 June 10-13*Federal Aviation Administration, Chicago, IL.

[17] S. Zelinski, "A comparison of algorithm generated sectorizations," *Air Traffic Control Quarterly*, vol. 18, no. 3, pp. 279–301, 2010.

[18] D. Delahaye and S. Puechmorel, "3D airspace sectoring by evolutionary computation: real-world applications," in *Proceedings of the 8th annual conference on Genetic and evolutionary computation*, pp. 1637–1644, Seattle, Washington, USA, 2006.

[19] R. Kicinger and A. Yousefi, "Heuristic method for 3D airspace partitioning: genetic algorithm and agent-based approach," in *9th AIAA Aviation Technology, Integration, and Operations Conference (ATIO)*, Hilton Head, South Carolina, 2009.

[20] J. Tang, S. Alam, C. Lokan, and H. A. Abbass, "A multi-objective evolutionary method for dynamic airspace re-sectorization using sectors clipping and similarities," in *2012 IEEE Congress on Evolutionary Computation*, pp. 1–8, Brisbane, QLD, Australia, 2012.

[21] J. Tang, S. Alam, C. Lokan, and H. A. Abbass, "A multi-objective approach for dynamic airspace sectorization using agent based and geometric models," *Transportation research part C: Emerging technologies*, vol. 21, no. 1, pp. 89–121, 2012.

[22] M. Xue, "Three-dimensional sector design with optimal number of sectors," *Journal of Guidance, Control, and Dynamics*, vol. 35, no. 2, pp. 609–618, 2012.

[23] J. Wei, V. Sciandra, I. Hwang, and W. D. Hall, "Design and evaluation of a dynamic sectorization algorithm for terminal airspace," *Journal of Guidance, Control, and Dynamics*, vol. 37, no. 5, pp. 1539–1555, 2014.

[24] M. Sergeeva, D. Delahaye, and C. Mancel, "3D airspace sector design by genetic algorithm," in *2015 International Conference on Models and Technologies for Intelligent Transportation Systems (MT-ITS)*, pp. 499–506, Budapest, Hungary, 2015.

[25] C. Yin, T. K. Venugopalan, and S. Suresh, "A multi-objective approach for 3D airspace sectorization: a study on Singapore regional airspace," in *2016 IEEE Symposium Series on Computational Intelligence (SSCI)*, pp. 1–8, Athens, Greece, 2016.

[26] C. Schmidt, T. A. Granberg, T. Polishchuk, and V. Polishchuk, "Convex sectorization—a novel integer programming approach," in *2017 Integrated Communications, Navigation and Surveillance Conference (ICNS)*, pp. 1–124, Herndon, VA, USA, 2017.

[27] T. A. Granberg, T. Polishchuk, V. Polishchuk, and C. Schmidt, "Integer programming–based airspace sectorization for terminal maneuvering areas with convex sectors," *Journal of Air Transportation*, vol. 27, no. 4, pp. 169–180, 2019.

[28] H. Oktal, K. Yaman, and R. Kasımbeyli, "A mathematical programming approach to optimum airspace sectorisation problem," *Journal of Navigation*, vol. 73, no. 3, pp. 599–612, 2020.

[29] P. Kopardekar, K. Bilimoria, and B. Sridhar, "Initial concepts for dynamic airspace configuration," in *7th AIAA ATIO Conf, 2nd CEIAT Int'l Conf on Innov and Integr in Aero Sciences,17th LTA Systems Tech Conf; followed by 2nd TEOS Forum*, Belfast, Northern Ireland, 2007.

[30] S. A. Martinez, G. B. Chatterji, D. Sun, and A. Bayen, "A weighted-graph approach for dynamic airspace configuration," in *AIAA Guidance, Navigation and Control Conference and Exhibit*, Hilton Head, South Carolina, 2007.

[31] G. R. Sabhnani and L. Martin, *Geometric Algorithms for Dynamic Airspace Sectorization*, State University of New York at Stony Brook, 2009.

[32] Y. Chen, H. Bi, D. Zhang, and Z. Song, "Dynamic airspace sectorization via improved genetic algorithm," *Journal of Modern Transportation*, vol. 21, no. 2, pp. 117–124, 2013.

[33] M. Schultz, I. Gerdes, T. Standfuß, and A. Temme, "Future airspace design by dynamic sectorization," in *Lecture Notes in Electrical Engineering*, pp. 19–34, Springer, Singapore, 2019.

[34] T. K. Venugopalan, C. S. Y. Wong, S. Suresh, and N. Sundararajan, "Simultaneous optimization of airway and sector design for air traffic management," *Journal of Air Transportation*, vol. 26, no. 1, pp. 8–22, 2018.

[35] I. Gerdes, A. Temme, and M. Schultz, "Dynamic airspace sectorisation for flight-centric operations," *Transportation Research Part C: Emerging Technologies*, vol. 95, pp. 460–480, 2018.

[36] C. Wong, S. Sundaram, and N. Sundararajan, "CDAS: a cognitive decision-making architecture for dynamic airspace sectorization for efficient operations," *IEEE Transactions on Intelligent Transportation Systems*, vol. 20, no. 5, pp. 1659–1668, 2019.

[37] C. Wong, S. Suresh, and N. Sundararajan, "A rolling horizon optimization approach for dynamic airspace sectorization," *IFAC Journal of Systems and Control*, vol. 11, article 100076, 2020.

[38] C. Chen, J. Jiang, Y. Zhou, N. Lv, X. Liang, and S. Wan, "An edge intelligence empowered flooding process prediction using Internet of things in smart city," *Journal of Parallel and Distributed Computing*, vol. 165, pp. 66–78, 2022.

[39] J. Huang, H. Gao, S. Wan, and Y. Chen, "AoI-aware energy control and computation offloading for industrial IoT," *Future Generation Computer Systems*, vol. 139, pp. 29–37, 2023.

[40] A. D. Boursianis, M. S. Papadopoulou, A. Gotsis et al., "Smart irrigation system for precision agriculture—the AREThOU5A IoT platform," *IEEE Sensors Journal*, vol. 21, no. 16, pp. 17539–17547, 2021.

[41] X. Deng, Z. Sun, D. Li, J. Luo, and S. Wan, "User-centric computation offloading for edge computing," *IEEE Internet of Things Journal*, vol. 8, no. 16, pp. 12559–12568, 2021.

[42] S. J. Corrado, T. G. Puranik, O. J. Pinon, and D. N. Mavris, "Trajectory clustering within the terminal airspace utilizing a weighted distance function," in *8th OpenSky Symposium 2020*, vol. 59no. 1, p. 7, Brussels, Belgium, 2020.

[43] Z. Wang, M. Liang, and D. Delahaye, "A hybrid machine learning model for short-term estimated time of arrival prediction in terminal manoeuvring area," *Transportation Research Part C: Emerging Technologies*, vol. 95, pp. 280–294, 2018.

[44] R. Sun, J. Li, K. Niu, Y. Tian, and C. Xu, "Research on joint ground movement optimization based on bilevel programming," *Aerospace*, vol. 9, no. 9, p. 502, 2022.